



Subthalamic nucleus deep brain stimulation for cranial-cervical dystonia: optimal stimulation sites and networks

Hutao Xie ^a, Jiansong Huang ^a, Ningfei Li ^b, Houyou Fan ^a, Shihang Yang ^c, Zixiao Yin ^a, Zhaoting Zheng ^a, Zehua Zhao ^a, Yin Jiang ^{d,e}, Lin Shi ^a, Anchao Yang ^a, Fangang Meng ^{a,d}, Guanyu Zhu ^{a,*}, Quan Zhang ^{a,**}, Jianguo Zhang ^{a,d,e,***}

^a Department of Neurosurgery, Beijing Tiantan Hospital, Capital Medical University, Beijing, China

^b Movement Disorders and Neuromodulation Unit, Department of Neurology, Charité-Universitätsmedizin Berlin, Berlin, Germany

^c School of Electronics Engineering and Computer Science, Peking University, Beijing, China

^d Department of Functional Neurosurgery, Beijing Neurosurgical Institute, Capital Medical University, Beijing, China

^e Beijing Key Laboratory of Neurostimulation, Beijing, China

ARTICLE INFO

Keywords:

Cranial-cervical dystonia
Meige syndrome
Deep brain stimulation
Subthalamic nucleus
Connectome

ABSTRACT

Background and objectives: Deep brain stimulation (DBS) of the subthalamic nucleus (STN) is an effective treatment for medically refractory cranial-cervical dystonia (CCD or Meige syndrome). However, clinical responses vary substantially across individuals, likely due to differences in electrode placement and modulation of target neural circuits.

Methods: We retrospectively analyzed 51 patients with CCD treated with STN-DBS at a single center. Pre- and postoperative imaging was used to reconstruct electrode locations and model patient-specific electric fields. We then performed (i) voxel-wise sweet spot mapping to identify optimal stimulation sites, (ii) fiber filtering using normative tractography to determine white matter pathways associated with clinical improvement, and (iii) network mapping based on resting-state fMRI to identify functional connectivity patterns predictive of DBS response.

Results: Voxel-wise correlation analysis revealed that the optimal stimulation localized to the STN motor subregion ($R = 0.52, p < 0.001$). Normative structural connectivity analysis showed that symptom improvement correlated strongly with modulation of fibers projecting to the cranial and cervical regions of sensorimotor cortex ($R = 0.52, p < 0.001$) and sensorimotor-associated basal ganglia pathways ($R = 0.62, p < 0.001$). Functional network mapping further revealed connectivity to the sensorimotor cortex as significantly associated with clinical improvement ($R = 0.43, p = 0.002$).

Conclusion: These findings inform refinement of STN targeting strategies in DBS for CCD. The involvement of cranial and cervical sensorimotor regions highlights the importance of symptom-based dystonia classification for individualized neuromodulation approaches.

1. Introduction

Cranial-cervical dystonia (CCD), also called Meige syndrome, is a focal dystonia characterized by involuntary muscle contractions, typically affecting the eyelids (blepharospasm), jaw and lower facial muscles (oromandibular dystonia) [1]. Standard treatments include oral anti-cholinergics and botulinum toxin injections, while deep brain

stimulation (DBS) is considered for medication-refractory cases [2]. Historically, the globus pallidus internus (GPI) has been the primary DBS target supported by substantial evidence of safety and efficacy [3,4]. More recently, the subthalamic nucleus (STN) has emerged as a promising alternative target, as shown in our prior work and other studies [5, 6]. STN-DBS offers comparable therapeutic benefits with additional advantages, including improved visualization T2-weighted MRI,

* Corresponding author. The South Fourth Ring Road, West Road, Fengtai District & No. 119, Beijing, 100070, China.

** Corresponding author. The South Fourth Ring Road, West Road, Fengtai District & No. 119, Beijing, 100070, China.

*** Corresponding author. The South Fourth Ring Road, West Road, Fengtai District & No. 119, Beijing, 100070, China.

E-mail addresses: zhuguanyu1991@ccmu.edu.cn (G. Zhu), quanzhang0110@163.com (Q. Zhang), zjguo73@126.com (J. Zhang).

reduced battery consumption, and faster therapeutic onset [7,8].

Despite these advances, clinical outcomes following STN-DBS in CCD have shown considerable variability. Therapeutic efficacy critically depends on precise electrode placement and meticulous postoperative programming [9]. Earlier studies, including ours, have demonstrated that greater overlap between the volume of tissue activated (VTA) and the dorsolateral subregion of the STN is associated with better motor outcome [8–10]. However, these findings relied on volumetric overlap analyses and lacked voxel-level spatial precision. This limitation is particularly relevant given the anatomical complexity of the STN, which is traversed by multiple fiber tracts and bordered by distinct gray matter structures [11]. To date, no study has delineated the voxel-level “sweet spot” for STN-DBS specifically in CCD. Moreover, while STN targeting is clinically effective, the underlying white matter tracts and functional networks mediating this benefit remain poorly understood.

Recent connectomic DBS studies have provided valuable mechanistic insights into dystonia. Horn et al. [12] mapped distinct GPI sweet spots, symptom-specific fiber tracts, and a shared cerebellar - somatomotor network across a large cohort of cervical and generalized dystonia patients. Building on this framework, Butenko et al. [13] performed multi-level connectomic mapping in a heterogeneous STN-DBS cohort stratified by symptom predominance. In that study, patients were categorized by symptom region (e.g., blepharospasm, cervical, appendicular), and a single individual could be represented multiple times. While informative, their approach may introduce potential overlap and confounds, particularly in cases of multifocal dystonia involving multiple anatomical regions, thereby limiting phenotype specificity.

To address these gaps, we conducted a comprehensive voxelwise and connectomic analysis based on the same well-characterized cohort of 51 CCD patients previously reported in our outcome study. Specifically, we applied sweet spot mapping, fiber filtering, and whole-brain network analysis based on electric field (E-field) modeling [14]. To our knowledge, this is the first systematic investigation of optimal stimulation sites and therapeutic network mechanisms of STN-DBS specifically in CCD. Our aims were to (i) identify optimal stimulation sites at the voxel level, (ii) delineate white matter pathways modulated by effective stimulation, and (iii) characterize distributed functional networks associated with clinical improvement.

2. Methods

2.1. Standard protocol approvals, registrations, and patient consent

This study was approved by the Institutional Research Ethics Board of Beijing Tiantan Hospital, Capital Medical University (IRB No. KY2022-073-02). Written informed consent was obtained from all patients.

2.2. Patient selection

We included consecutive patients diagnosed with CCD [15] who underwent bilateral STN-DBS at Beijing Tiantan Hospital between January 2016 and June 2023. Detailed inclusion and exclusion criteria have been described previously [8].

2.3. Imaging acquisition, pre-processing, and electrode localization

Preoperative structural MRI (1 mm isotropic) was acquired using a 3.0T scanner. Postoperative CT scans were obtained at a slice thickness of 0.625 mm. Electrodes localization was performed using Lead-DBS v3.1 (<https://www.lead-dbs.org>) [14]. Briefly, postoperative CT images were linearly co-registered to preoperative MR using the Advanced Normalization Tools (ANTs, <http://stnava.github.io/ANTs/>) [16]. All co-registered images were visually inspected by two experienced users. In one patient, minor residual misalignment was observed after automatic co-registration (Supplementary Fig. 1). To ensure precise

electrode localization, manual refinement was performed using 3D Slicer (www.slicer.org) [17]. Brain shift correction was then applied to account for potential pneumocephalus [17]. Preoperative images were normalized to the ICBM 2009b Nonlinear Asymmetric (“MNI”) space using the SyN algorithm in ANTs, with the “effective: low variance + subcortical refinement” preset in Lead-DBS [18]. This multi-spectral normalization method has shown spatial accuracy comparable to expert manual segmentation [19,20]. Electrodes were initially localized from postoperative CT using the phantom-validated PaCER algorithm [21], followed by visual inspection and manually refined by two experienced users. Image segmentation was performed using the DISTAL atlas [22,23], and group-level visualizations were generated with the Lead-Group toolbox [14].

2.4. E-field modeling

Patient-specific E-field distributions were estimated in native space using the SimBio/FieldTrip pipeline (<http://fieldtriptoolbox.org/>) [24] as implemented in Lead-DBS. This approach solves the quasi-static form of Maxwell’s equations (specifically, the Laplace equation) via the Finite Element Method (FEM), modeling the head as a tetrahedral mesh comprising four compartments with defined electrical conductivities: gray matter (0.33 S/m), white matter (0.14 S/m), electrode contacts (10^8 S/m), and insulating parts (10^{-16} S/m) [25]. Patient-specific DBS settings (e.g., active contact configuration, voltage) were used to define the boundary conditions (Fig. 1a). The spatial gradient of the voltage field was computed to obtain the E-field vector at each voxel, and the scalar magnitude of this vector was used as the basis for downstream sweet spot, fiber, and network analyses. Only scalar magnitudes were analyzed; directional (vectorial) information was not incorporated [14].

As clinical outcomes were evaluated under bilateral stimulation, we followed prior dystonia studies [12,13,26], that assumed mirrored stimulation yields comparable effects across hemispheres. Accordingly, stimulation sites were mirrored between hemispheres to allow pooled group-level modeling. This approach enabled pooling of all 102 hemispheric E-fields (2 per patient) into a unified analysis framework in MNI space. Where applicable, a threshold of 0.2 V/mm was applied to derive binary stimulation volumes, based on established axonal activation thresholds.

2.5. Sweet spot mapping

Sweet spot mapping [27] (Fig. 1b) was performed to identify subthalamic voxels associated with optimal clinical improvement. For each voxel covered by the group-level E-fields in MNI space, Spearman correlation coefficient was calculated between E-field magnitude across subjects and clinical improvement, as assessed by the Burke-Fahn-Marsden Dystonia Rating Scale-movement (BFMDRS-M). To reduce bias from sparsely covered voxels and enhance result reliability, analysis was restricted to voxels encompassed by at least 50 % of E-fields exceeding 0.2 V/mm, an activation threshold commonly used to model DBS effects [25,28,29].

2.6. Fiber filtering

Fiber filtering (Fig. 1c) was performed to identify DBS-intersected pathways associated with clinical improvement. For each subject, fibers traversing E-field voxels were projected into MNI space [30]. Normative structural connectivity was derived from two sources: a population-based group connectome from multi-shell dMRI-based tractography of 985 healthy participants (from the HCP 1200 subjects release) [30], and a predefined set of 28,600 subcortical tracts from the Basal Ganglia Pathway Atlas [31]. Each fibers was weighted by the E-field magnitude across all traversed voxels. Only fibers intersecting >20 % of stimulation volumes with an E-field magnitude >0.40 V/mm were included. Spearman correlation coefficients were then calculated

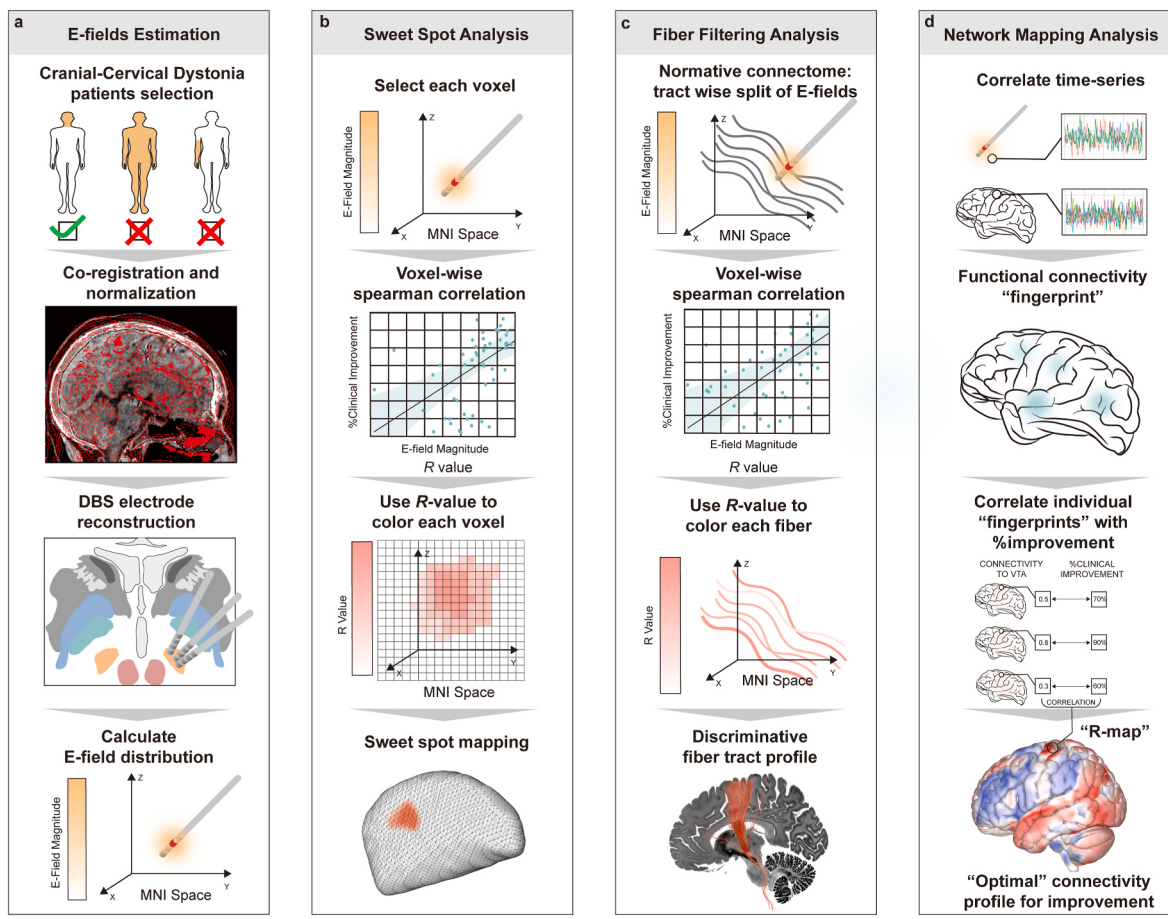


Fig. 1. | Outline of methods applied.

a, E-fields estimation. Consecutive cranial-cervical dystonia (CCD) patients were recruited and enrolled according to preset inclusion criteria. Postoperative CT scans were co-registered with preoperative MRI using ANTs in Lead-DBS. All registrations were visually inspected, and in one case with minor residual misalignment, manual refinement was performed using 3D Slicer to ensure accurate electrode localization (see *Supplementary Fig. 1*). Electrode trajectories were then reconstructed in Montreal Neurological Institute (MNI) space [88]. The electric field vector (E-field) represents the first derivative of the estimated voltage distribution across MNI voxels, with maximal intensity near active contacts and rapid decay with distance.

b, Sweet spot analysis. Based on E-field estimates, voxel-wise Spearman correlations were calculated between %BFMDRS-M improvement and the E-field magnitude for each electrode. Correlation coefficients (R values) were mapped onto an ultrahigh-resolution human brain template, with hot colors representing positively correlated voxels ($R > 0$).

c, Fiber filtering analysis. E-field values at each fiber segment were calculated using the same estimates as in panel a. The association between fiber modulation and clinical improvement was assessed by rank correlation, and R values were projected onto the brain template, with hotter colors indicating stronger correlations.

d, Network mapping analysis. Functional connectivity maps were generated from a normative dataset of 1000 healthy individuals [89]. Voxel-wise correlations between E-field connectivity profiles and clinical improvement were computed to construct an R-map reflecting the optimal therapeutic network.

between fiber weights and the clinical improvement (%BFMDRS-M improvement) across the subjects, with higher R-value indicating stronger associations with motor improvement. To assess robustness, fiber filtering was repeated using different thresholds for the proportion of high-intensity E-field coverage (>0.40 V/mm) per fiber. This method has demonstrated consistent predictive utility across DBS cohorts with various indications [32–35].

2.7. Network mapping

Network mapping (Fig. 1d) was performed to characterize the functional connectivity profiles associated with patient-specific DBS stimulation sites. For each patient, the corresponding E-field magnitude distribution was used as a region of interest (ROI) to seed functional connectivity analysis within a normative resting-state fMRI connectome derived from 1000 healthy individuals (Brain Genomics Superstruct Project) [36]. The mean BOLD time series across each ROI was extracted and correlated with time series from all other brain voxels. The individual correlation maps were Fisher z-transformed and averaged across

subjects to generate a whole-brain connectivity fingerprint per patient. Next, voxel-wise Spearman correlations were computed across patients between connectivity strength and clinical improvement, yielding an R-map representing the optimal connectivity profile associated with therapeutic response.

To assess the robustness of the resulting topographic maps, we applied voxelwise correction for multiple comparisons using the False Discovery Rate (FDR) method ($\alpha = 0.05$). Significant clusters were interpreted as regions whose functional connectivity with the stimulation site correlated with clinical outcome.

2.8. Statistical analysis

Sweet-spot mapping, fiber filtering, and network mapping were initially conducted using a mass-univariate design. To assess the robustness and generalizability of the resulting spatial models, we applied leave-one-patient-out (LOO), 10-fold, 7-fold, and 5-fold cross-validation (CV) paradigms.

In each iteration, a subset of patients was held out before any

analysis. Spatial models (e.g., sweet spot maps, fiber R-maps) were then recalculated using only the remaining training patients. Prediction scores for held-out patients were computed by correlating their E-fields or connectivity maps with the training-derived model. For LOO, this process was repeated 51 times, once per patient. For k-fold CV, the cohort was randomly split into k parts, with each part serving as test data once. Prediction performance was measured by correlating predicted scores with observed clinical improvements across all patients. To adjust for known confounders, preoperative BFMDRS-M scores and disease duration were included as covariates in all validations [8]. One-sided tests were applied, as we expected only positive associations.

To quantify the possibility of a type I error, we used permutation testing for the network mapping model (1000 iterations). In each iteration, clinical scores were randomly reassigned across patients to generate null R-maps. We compared the original (unpermuted) model's peak R-value to this null distribution, with $p < 0.05$ considered significant.

3. Results

3.1. Patients and clinical outcomes

This post hoc analysis included 51 patients (mean age at surgery: 55.7 ± 9.7 years, mean disease duration: 5.2 ± 4.5 years, 33 females) with medication-refractory CCD who underwent bilateral STN-DBS (L301, PINS Medical Co. Ltd., or 3389, Medtronic). In this previously described cohort, mean stimulation parameters were 2.71 ± 0.63 V, 139.02 ± 20.46 Hz, and 76.67 ± 26.66 μ s. At the final follow-up (27.31 ± 18.00 months), BFMDRS-M scores decreased from 12.9 ± 5.2 at baseline to 5.3 ± 4.2 , representing a 58.9 % improvement ($p < 0.001$). Demographic and clinical outcomes are summarized in Table 1. Individual-level data were published previously [8]. Reconstructed DBS electrodes are shown in Fig. 2. Most active contacts were located within the STN, with some extending into adjacent regions such as the zona incerta.

3.2. Optimal DBS site for CCD (sweet spot analysis)

Voxel-wise Spearman correlation analysis between E-field distribution (visualized on the 7T Ex vivo 100 mm Brain Atlas [37]) and

Table 1
Demographic characteristics and STN-DBS outcomes of 51 individuals with cranial-cervical dystonia.

Characteristics	Pre-operation assessment	Post-operation assessment	Paired t-test <i>p</i> value
Demographical Characteristics			
Sex (Male)	18 (35.29 %)		
Disease duration (years)	5.17 ± 4.46		
Onset age (years)	50.55 ± 9.29		
Age at surgery (years)	55.71 ± 9.74		
Follow up (months)	27.31 ± 18.00		
Clinical assessments			
BFMDRS-M	12.93 ± 5.18	5.25 ± 4.22	<0.001
Eye score	6.58 ± 1.68	2.47 ± 2.25	<0.001
Mouth score	3.63 ± 2.38	1.48 ± 1.85	<0.001
Swallow/Speech score	1.86 ± 2.14	0.83 ± 1.08	<0.001
Neck score	0.86 ± 1.75	0.47 ± 0.83	0.026
Stimulation parameters			
Voltage (V)		2.71 ± 0.63	
Pulse width (μ s)		76.67 ± 26.66	
Frequency (Hz)		139.02 ± 20.46	

Abbreviations: BFMDRS-M, Burke-Fahn-Marsden Dystonia Rating Scale-movement.

BFMDRS-M score improvement localized the sweet spot to the motor subregion of the STN (peak $R = 0.77$) (Fig. 3a and b), specifically the cranial and cervical motor region of the STN described by Nambu [38] (Fig. 3c). The MNI coordinates of sweet spots are listed in Supplementary Table 1. Similar results were obtained after adjusting for disease duration and baseline BFMDRS-M score as covariates (Supplementary Fig. 1). The model's robustness was confirmed by LOO ($R = 0.52$, $p = 4.0 \times 10^{-4}$), 10-fold ($R = 0.58$, $p = 2.0 \times 10^{-4}$), 7-fold ($R = 0.56$, $p = 2.0 \times 10^{-4}$), and 5-fold ($R = 0.51$, $p = 4.0 \times 10^{-4}$) cross-validation (Fig. 3d and Supplementary Fig. 3), with consistent results after covariate adjustment (Supplementary Fig. 4).

3.3. Spatial trajectory of white matter tracts associated with optimal DBS response (fiber filtering analysis)

Using the HCP-985 connectome [30], we constructed a model of white matter pathways traversing STN-DBS E-fields. Streamlines projected to the prefrontal cortex, supplementary motor area (SMA), premotor area, somatosensory cortex, and primary motor cortex (M1) (Fig. 4a and b). Tracts connecting the STN to the sensorimotor cortex and SMA showed strongest association with clinical improvement. Based on qualitative visual inspection, these optimal-outcome-associated tracts appeared to project predominantly to the cranial and cervical representations of the sensorimotor cortex, in line with homuncular topography (Fig. 4c). Similar patterns were observed after adjusting for preoperative BFMDRS-M scores and disease duration (Supplementary Fig. 5). The structural model was validated using LOO ($R = 0.52$, $p = 6.0 \times 10^{-4}$), 10-fold ($R = 0.61$, $p = 2.0 \times 10^{-4}$), 7-fold ($R = 0.54$, $p = 2.0 \times 10^{-4}$), and 5-fold ($R = 0.58$, $p = 2.0 \times 10^{-4}$) cross-validation (Fig. 4d, Supplementary Fig. 6). Covariate-adjusted models yielded comparable performance (Supplementary Fig. 7). Varying the E-field voxel threshold (0.4 V/mm) did not alter streamline distribution (Supplementary Fig. 8).

We further replicated the analysis using the Basal Ganglia Pathway Atlas [31]. Consistent with the HCP-based results, tracts associated with optimal outcomes were primarily localized within motor-related regions (Fig. 5), stable after covariate adjustment (Supplementary Fig. 9). This model was also validated across all CV schemes ($R = 0.57\text{--}0.63$, $p < 0.001$, Supplementary Figs. 10 and 11).

3.4. Distributed functional whole-brain networks associated with optimal DBS response (network mapping analysis)

While sweet spot and fiber analyses reflect local and tract level effects of DBS, they do not capture distributed network-level associations with clinical outcome. To address this, we performed DBS network mapping. After voxelwise FDR correction, greater connectivity between stimulation sites and the sensorimotor cortex was significantly associated with clinical improvement, whereas higher connectivity to the dorsomedial prefrontal cortex/anterior cingulate cortex, dorsolateral prefrontal cortex, and posterior cingulate cortex was linked to poorer outcomes (Fig. 6a; Supplementary Tables 2 and 3).

Model robustness was supported by LOOCV ($R = 0.46$, $p = 0.001$) and permutation testing ($R = 0.43$, $p = 0.002$; Fig. 6b), and further tested via 10-fold ($R = 0.35$, $p = 0.014$) and 7-fold ($R = 0.27$, $p = 0.059$, Supplementary Fig. 12) CV. After adjusting for disease duration and baseline BFMDRS-M scores, the model remained stable with LOOCV ($R = 0.34$, $p = 0.017$, Supplementary Figs. 13 and 14).

4. Discussion

Precise targeting and understanding of underlying networks are critical for optimizing the therapeutic efficacy of STN-DBS in CCD. In this study, we performed a comprehensive multi-level connectomic analysis in a well-characterized cohort of CCD patients, revealing key anatomical and network-level substrates associated with clinical improvement. First, we identified an optimal stimulation site located

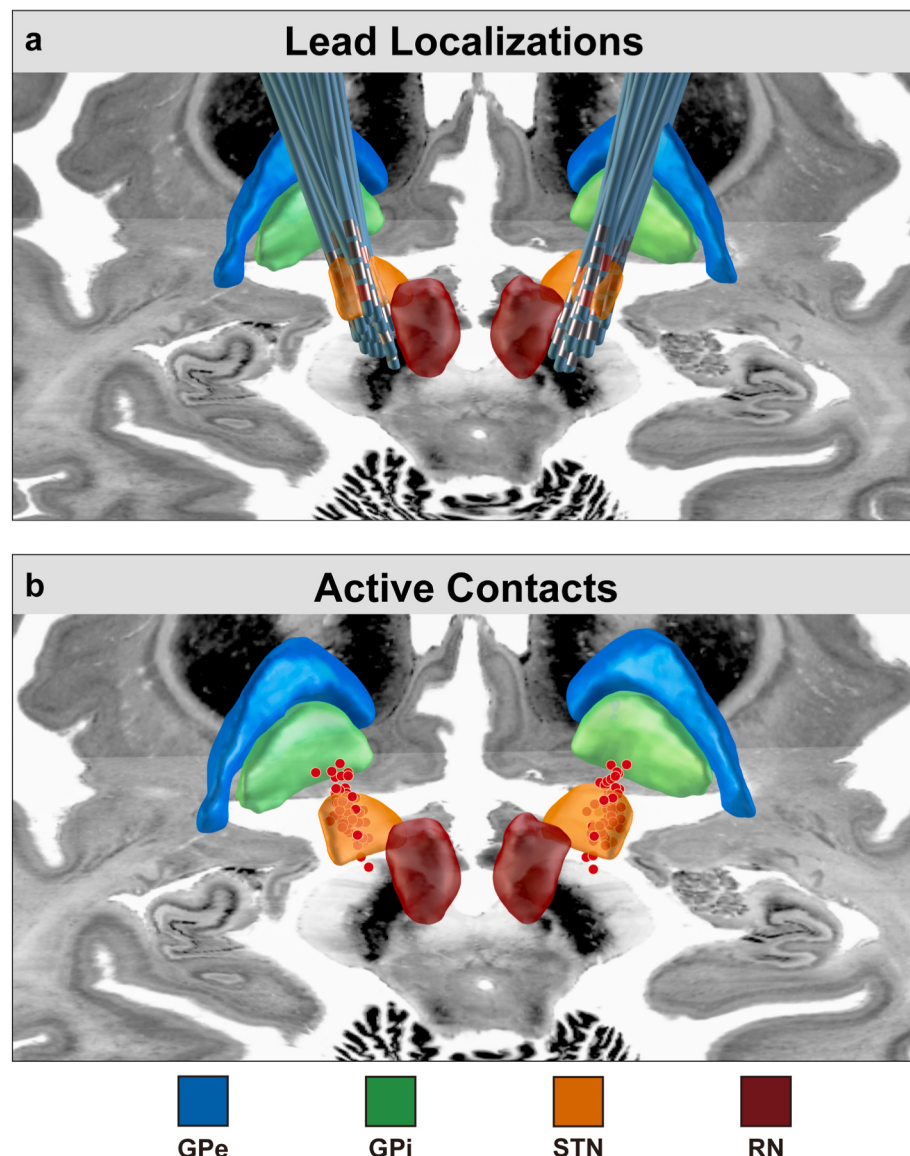


Fig. 2. | Anatomical distribution of DBS electrodes at the mesencephalic level.

a, Reconstruction of DBS electrode placement.

b Active contacts visualized as red spots. Electrodes and other relevant structures are overlaid on an the 7T ex vivo 100- μ m human brain template [89].

Abbreviations: STN, Subthalamic Nucleus; GPe, Globus Pallidus Externus; GPI, Globus Pallidus Internus; RN, Red Nucleus.

within the posterodorsolateral STN. Second, we provide evidence that a hyperdirect pathway linking the STN to the somatotopic representation of the cranial and cervical regions of sensorimotor cortex and SMA. In addition, the indirect pathway also involving the STN motor subregion also emerged as a therapeutically relevant circuit. Third, we identify a specific pattern of functional connectivity with STN-DBS correlates with clinical outcome across patients in CCD.

Given that “millimeters matter” in DBS electrode placement, especially when targeting small and heterogeneous structures like the STN, these findings may help refine surgical targeting and postoperative programming strategies in CCD. Furthermore, the observation that optimal stimulation sites are connected to cortical regions representing symptomatic body areas emphasizes the importance of accurate clinical phenotyping to guide individualized neuromodulation approaches.

4.1. Optimal stimulation sites in STN-DBS for CCD

Previous literatures, including our own, reported correlations

between better clinical outcomes and greater overlap between the VTA and the dorsolateral (sensorimotor) subregion of the STN in patients with CCD [8–10]. However, these studies primarily relied on volumetric overlap analyses, which, although informative, lack the spatial precision required to pinpoint optimal stimulation site. Given the relatively large size and complex anatomical structure of the dorsolateral sensorimotor subregion of the STN compared to the scale of individual electrode contacts, different contacts may stimulate distinct portions of this region [39,40]. Therefore, coarse anatomical targeting alone may be insufficient to identify the most effective stimulation site for achieving maximal therapeutic benefit. To address this limitation, we conducted voxel-level sweet spot mapping in the largest known single-center cohort of CCD patients treated with STN-DBS to date. Our analysis localized the optimal stimulation site within the somatotopic representation of the cranial and cervical sensorimotor regions of the STN [41]. This localization aligns directly with the clinical manifestations of CCD, which predominantly affect the cranial and cervical musculature. In support of this, previous studies on GPI-DBS have demonstrated

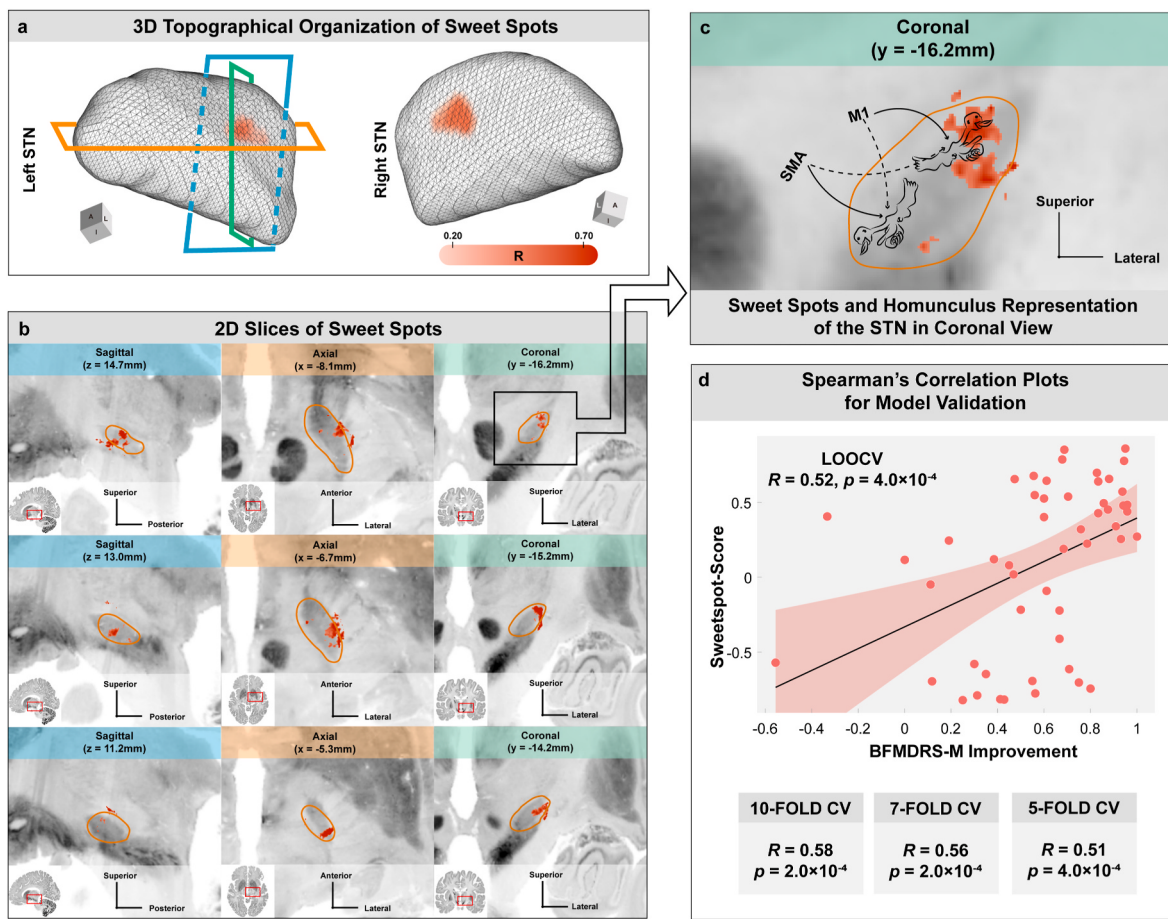


Fig. 3. | Optimal subthalamic stimulation site ('sweet spot') for cranial-cervical dystonia.

a, 3D topographical distribution of sweet spots projected as a density cloud on the subthalamic nucleus (STN) surface model in MNI space. Sweet spots were localized to the posterodorsolateral STN, visualized using a template STN surface from the DISTAL atlas [22].

b, Axial, coronal, and sagittal slices from the 7T ex vivo 100- μm human brain template showing voxelwise R-map results. Voxels positively associated with clinical improvement (BFMDRS-M) are shown in hot colors, confirming focal localization to the posterodorsolateral motor subregion of the STN.

c, Anatomical homuncular representation of the STN adapted from Nambu et al. [38] overlaid on the same 7T template. Neurons responsive to the orofacial, cervical, forelimb, and hindlimb regions of the motor cortex are positioned along the ventromedial-to-dorsolateral axis. Sweet spots predominantly align with the orofacial and cervical primary motor areas within this axis.

d, Model validation using cross-validation: LOOCV ($R = 0.52, p = 4.0 \times 10^{-4}$), 10-fold ($R = 0.58, p = 2.0 \times 10^{-4}$), 7-fold ($R = 0.56, p = 2.0 \times 10^{-4}$), and 5-fold ($R = 0.51, p = 4.0 \times 10^{-4}$). Each model was trained excluding test subjects and evaluated for prediction accuracy of clinical improvement.

Abbreviations: L, lateral side; A, anterior side; I, Inferior side.

somatotopic specificity in dystonia subtypes, including cervical and generalized dystonia [12], reinforcing the importance of anatomical precision in DBS targeting.

Moreover, recent research employing similar voxelwise techniques has identified distinct "sweet spots" for various dystonia symptoms, highlighting the symptom-specific nature of optimal stimulation sites [13]. Our results are consistent with these findings, as dorsolateral STN stimulation was shown to be optimal for appendicular dystonia and blepharospasm, while cervical dystonia exhibited a stronger response to stimulation targeting the ventral oral posterior nucleus of the thalamus. Discrepancy may be explained by the distinct pathophysiological mechanisms underlying various forms of dystonia [42]. Specifically, appendicular dystonia and blepharospasm primarily involve basal ganglia circuits and the hyperdirect motor cortical pathway projecting to the dorsolateral STN [43–46]. In contrast, cervical dystonia is linked to cerebellothalamic and brainstem networks projecting to thalamic motor nuclei, consistent with previous lesion studies implicating these regions [43,47,48]. These findings emphasize the need for precise, symptom-based targeting rather than generalized STN stimulation.

The emerging evidence supports the concept of phenotype-specific neuromodulation, where tailored stimulation strategies are employed

to address the unique neurophysiological characteristics of each dystonia subtype. Together, these results highlight the critical importance of individualized DBS targeting to optimize treatment outcomes across dystonia phenotypes.

4.2. Cortico-basal ganglia pathways modulation in CCD

In addition to motor dysfunction, patients with CCD often exhibit sensory impairments [1,49], including oral trauma [50], sensory tricks [51,52] and mirror movements [53]. These observations suggest that both sensory and motor components are involved in the pathophysiology and treatment of CCD. In this study, fiber filtering analysis revealed that effective stimulation intersected two major pathways: the hyperdirect pathway from cortex to STN [54,55] and subthalamic-pallidal fibers comprising the indirect pathway [56]. The basal ganglia act as an integrative hub, relaying diverse cortical inputs to the motor cortex to generate voluntary movement. Our findings showed that "sweet streamlines" predominantly involved projections from the sensorimotor cortex and SMA, consistent with the cranial and cervical distribution of symptoms in CCD.

The "hyperdirect pathway" is a cortico-subthalamic projection in

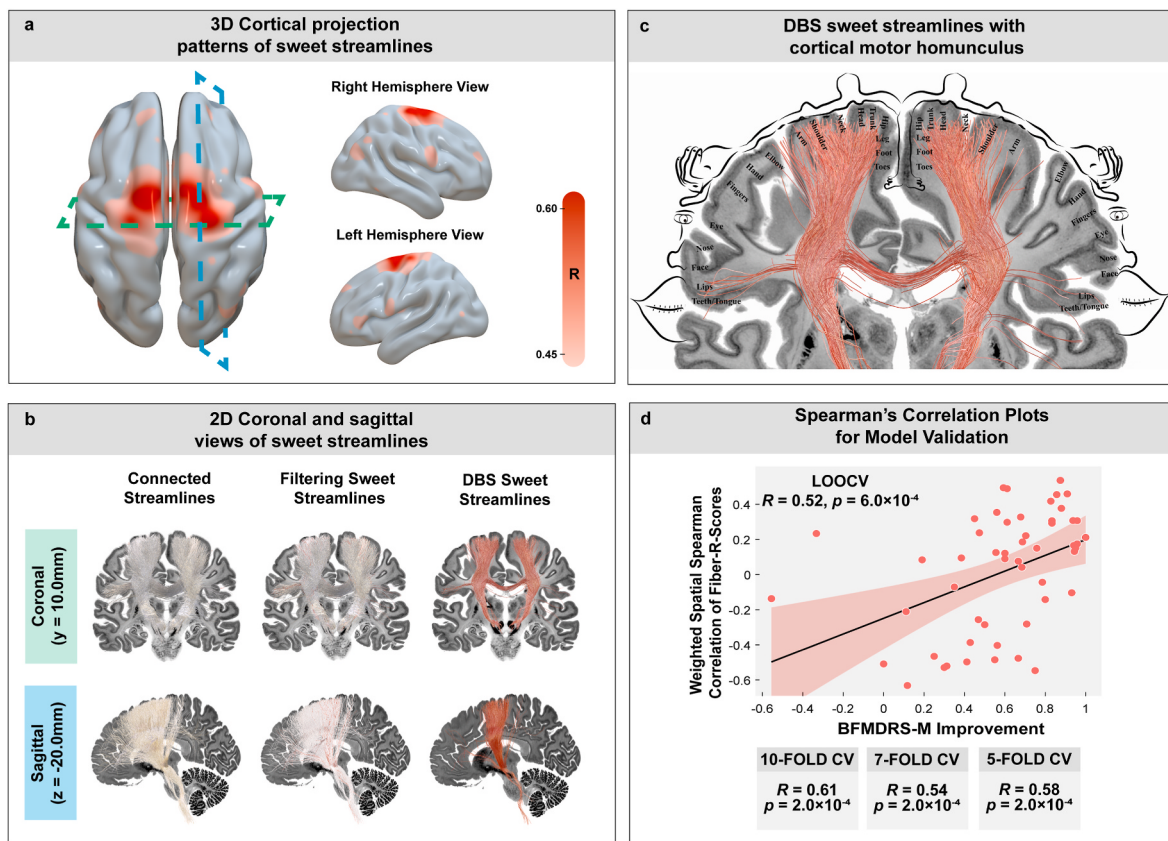


Fig. 4. | Topography of streamlines and interconnected cortical sites associated with therapeutic stimulation effects.

Structural connectivity analysis using fiber filtering to identify pathways connecting the STN with cortical regions significantly associated with motor improvement (%BFMDRS-M). Optimal streamlines were isolated from the HCP-985 normative group connectome; only fibers with Spearman's $R > 0.20$ are displayed (warmer colors indicate higher correlations).

- a, 3D cortical projections of sweet streamlines visualized on a transparent MNI template brain. Streamlines primarily target sensorimotor cortex regions.
- b, 2D stepwise fiber filtering analysis illustrated on coronal and sagittal slices of the 7T ex vivo 100- μm human brain template. Left column: all connected streamlines (white), defined as fibers intersecting $>20\%$ of stimulation volumes (E-field $>0.4\text{ V/mm}$). Middle column: filtering sweet streamlines, reflecting refinement towards streamlines strongly associated with clinical improvement. Right column: DBS sweet streamlines (red), the final subset significantly predictive of motor improvement.
- c, Coronal overlay of DBS sweet streamlines and the cortical motor homunculus, highlighting correspondence with cranial and cervical motor areas.
- d, Validation of the fiber filtering model using leave-one-out cross-validation (LOOCV; $R = 0.52, p = 6.0 \times 10^{-4}$), 10-fold ($R = 0.61, p = 2.0 \times 10^{-4}$), 7-fold ($R = 0.54, p = 2.0 \times 10^{-4}$), and 5-fold cross-validation ($R = 0.58, p = 2.0 \times 10^{-4}$). Each model was trained excluding test subjects and evaluated for prediction accuracy of clinical improvement.

Abbreviations: LOOCV, leave-one-out cross-validation.

which cortical neurons bypass the striatum and directly innervate the STN, establishing a fast and direct route by which the cortex can influence basal ganglia output [57]. Fibers correlated with clinical improvement were primarily connected to the cranial and cervical sensorimotor cortex and the SMA. By contrast, the indirect pathway comprises projections from the globus pallidus externus to the STN and from the STN to the GPi [58]. Although fibers modulated by DBS were distributed across all STN subregions, those associated with better outcomes were localized to the motor territory.

Previous neuroimaging [59–62] and electrophysiology [63,64] studies have implicated the sensorimotor, SMA and premotor components of cortico-basal ganglia pathways in CCD pathogenesis, primarily based on differences between patients and healthy controls [65]. More recent work has used symptom-based stratification to identify tracts associated with clinical improvement in dystonia. Using similar fiber filtering methods, those studies reported that STN projections from M1 were particularly relevant for appendicular dystonia and blepharospasm [13]. Our study, focusing specifically on CCD, identified sensorimotor cortico-basal ganglia pathways correlating with therapeutic benefit. Although these findings do not establish causality, they are associated

with therapeutic response and may reflect disease-relevant networks. This interpretation aligns with the “dysfunctome” framework proposed by recent studies [11,66–68], which defines disrupted circuits that may be normalized through effective neuromodulation. While we use this term to contextualize these findings, we acknowledge that our results demonstrate correlation rather than direct evidence of dysfunction. Nonetheless, the convergence between our results and prior studies supports the emerging view that dystonia subtypes are underpinned by symptom-specific network topologies, with implications for individualized targeting in DBS.

Three major hypotheses have been proposed to explain human dystonia: loss of motor inhibition, impaired sensorimotor integration, and maladaptive neural plasticity [65]. The pathways associated with therapeutic response in our study involved the STN, sensorimotor cortex, and SMA. The sensorimotor area executes the input of sensory information and output of motor information, and exhibits both structural and functional differences between dystonia patients and healthy controls, as revealed by neuroimaging [11,69] and electrophysiology [70,71]. Furthermore, The SMA execute the function of sensorimotor integration and postural adjustments and locomotion [72–74]. Abnormal

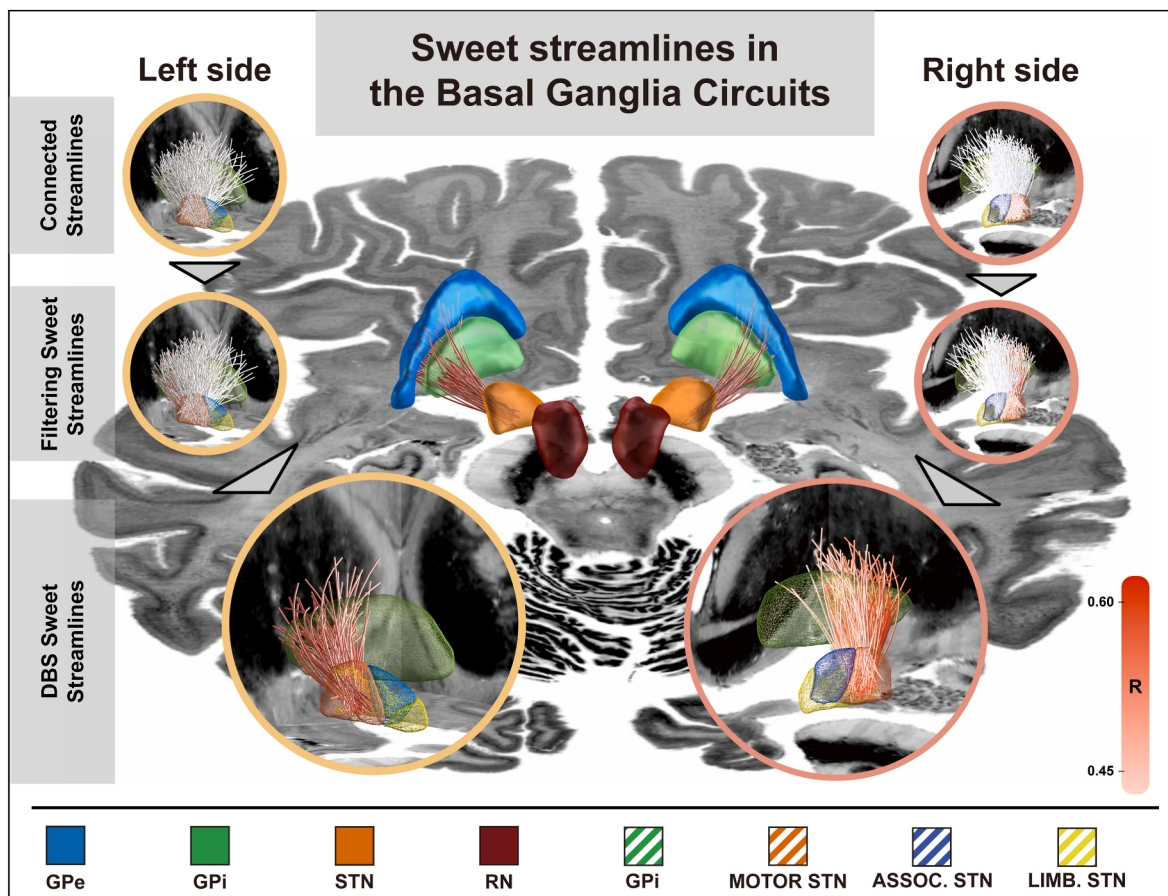


Fig. 5. | Structural connectivity of indirect pallido-subthalamic pathways associated with optimal DBS response.

This figure illustrates a stepwise fiber filtering analysis targeting indirect pallido-subthalamic pathways connecting the STN with the GPi and GPe, based on the Basal Ganglia Pathway Atlas [31].

Top row, connected streamlines (white) include fibers intersecting >20 % of stimulation volumes.

Middle row, filtering sweet streamlines represent a refined subset of connected streamlines, showing stronger correlations with clinical outcomes.

Bottom row, DBS sweet streamlines (red), the final subset significantly associated with motor improvement.

Streamlines are visualized bilaterally on a 3D axial view of the 7T ex vivo 100- μ m human brain template [89], along with basal ganglia nuclei segmentation from the DISTAL atlas [22]. Although DBS-modulated fibers spanned all functional STN subregions, DBS sweet streamlines primarily localized within the motor subregion. Abbreviations: MOTOR STN, motor subregion of STN; ASSOC. STN, associative subregion of STN; LIMB. STN, limbic subregion of STN.

SMA activity has been demonstrated in both patients [75,76] and animal models of dystonia [77,78], consistent with all three mechanistic hypotheses. These frameworks merit further investigation as unifying models across dystonia subtypes.

In addition, the different subtypes of dystonia also have unique characteristics that may stem for distinct impairments in cortical somatotopic representations. Thus, there may be a neuroanatomic as well as a clinical basis to classify dystonia and the former may be especially valuable for identifying optimal sites of invasive intervention or non-invasive therapeutic neuromodulation.

4.3. Potential contribution of cerebellar circuits to the dystonia network

Our structural and functional connectivity analyses aimed to identify circuits associated with STN-DBS efficacy in CCD. After correction for multiple comparisons, no cerebellar pathways were significantly correlated with clinical outcomes. Thus, our findings do not support a direct role for cerebellar connectivity in the therapeutic mechanism of STN-DBS.

Nevertheless, converging evidence from prior research suggests that the cerebellum may play a role in the broader pathophysiology of dystonia [79]. Neuroimaging studies have demonstrated cerebellar glucose hypometabolism [80], gray matter atrophy [81], and white matter

disruption [82] in CCD compared to healthy controls. Additionally, lesions in the cerebellopontine angle have been shown to induce secondary CCD [83]. Histopathological findings, such as reduced Purkinje cell density and synaptic changes in the dentate nucleus in postmortem blepharospasm cases, suggest microcircuit dysfunction that may impact motor control [84]. These findings are consistent with models of dystonia as a network disorder involving cortico-cerebello-thalamo-cortical loops [59,85,86].

Although not directly implicated in DBS response in this study, the cerebellum may serve a permissive or modulatory role within the dystonia network [13,48,87]. Future studies employing high-resolution cerebellar atlases, advanced tractography, or targeted neuro-modulation may better clarify its contribution to CCD and its treatment.

4.4. Clinical significance

Our findings provide practical insights for optimizing STN-DBS in CCD. First, precise targeting of the posterodorsolateral STN is critical for clinical benefit. Second, effective stimulation modulates fibers projecting to cranial and cervical sensorimotor regions, aligning with the symptom somatotopy of CCD. These findings support symptom-based targeting strategies. As shown in recent studies [13], blepharospasm and appendicular symptoms may respond best to dorsolateral STN

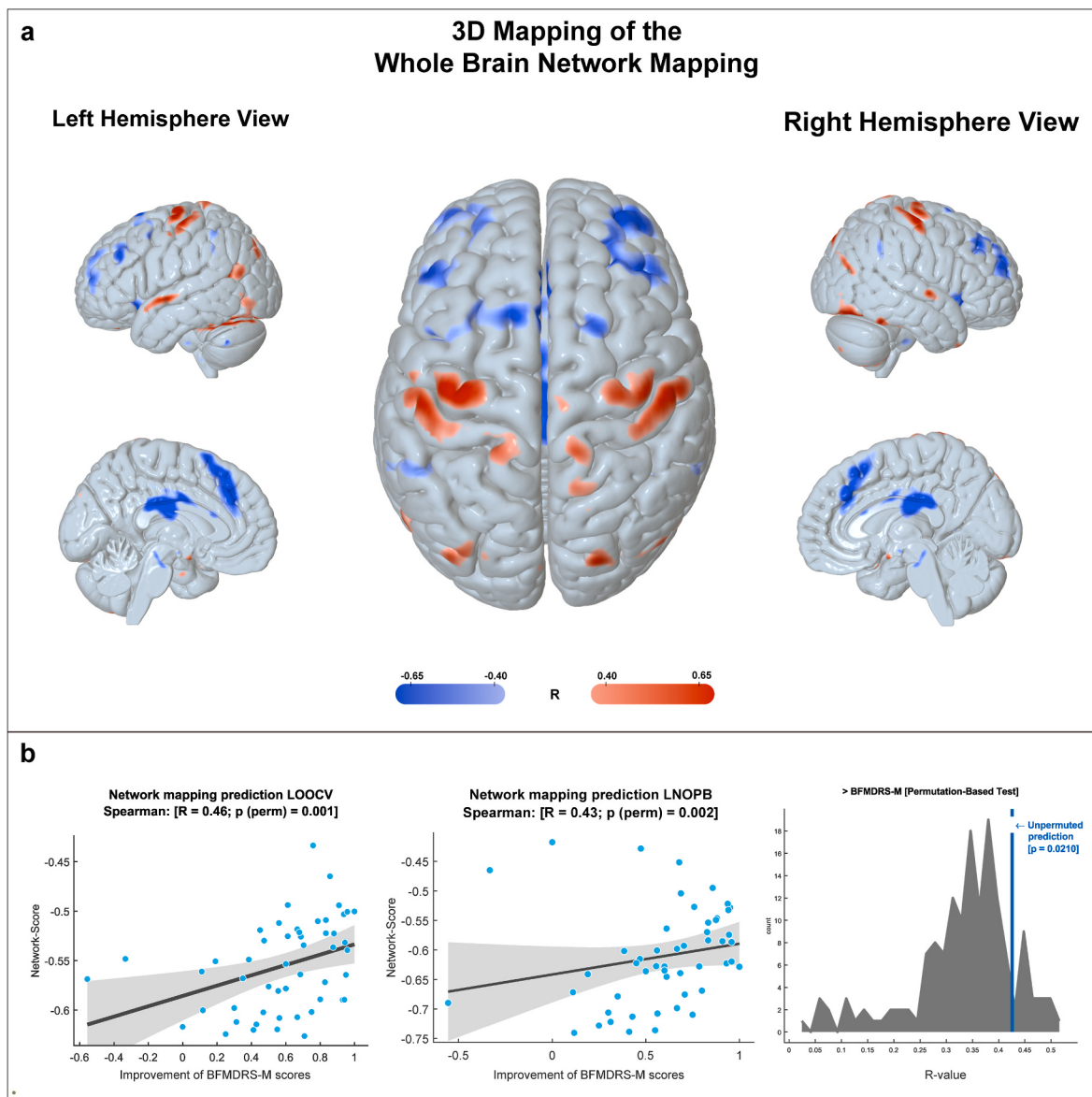


Fig. 6. | Whole-brain network mapping associated with therapeutic response to STN-DBS.
a, Network mapping results derived from normative resting-state fMRI data [36]. Warm-colored regions indicate areas whose stronger functional connectivity with stimulation sites was associated with better clinical outcomes, primarily involving the sensorimotor cortex. Cool-colored regions (e.g., MPFC, DLPFC, PCC) indicate areas where stronger connectivity correlated with poorer outcomes. Results are corrected by FDR methods ($\alpha < 0.05$).
b, Model validation using leave-one-patient-out cross-validation (LOOCV; $R = 0.46, p = 0.001$) and permutation testing ($R = 0.43, p = 0.021, 1000$ iterations). Each model was trained excluding test subjects and evaluated for prediction accuracy of clinical improvement.
Abbreviations: MPFC, medial prefrontal cortex; DLPFC, dorsolateral prefrontal cortex; PCC, posterior cingulate cortex.

stimulation, while cervical symptoms may benefit more from modulation near the ventral oral posterior nucleus. Such insights encourage the use of directional leads and individualized programming based on symptom distribution.

4.5. Limitations

This study has several limitations. First, the retrospective design precludes causal inference and limits adjustment for unmeasured covariates. However, the relatively large, single-center cohort may reduce clinical heterogeneity. We anticipate that future studies with larger samples and prospective designs will provide higher levels of clinical evidence.

Second, sweet spot mapping is limited to brain regions covered by E-fields exceeding a predefined threshold. It remains possible that more

effective stimulation sites exist outside this area, particularly those activated at lower thresholds. This limitation also applies to fiber filtering, where relevant tracts may be excluded if they are located in regions with subthreshold E-field intensity.

Third, structural and functional connectivity analyses were based on normative connectomes from healthy individuals. These reference datasets may not fully capture disease-specific brain alterations in dystonia. Although we employed a highly refined anatomical pathway atlas [31], some tracts or collaterals may be missing, which may limit anatomical completeness and interpretation. These results should therefore be considered hypothesis-generating and require validation with patient-specific imaging.

Fourth, in our voxel-wise functional connectivity analysis for network mapping, we employed FDR correction. Although commonly used, this method is known to be more susceptible to false positives

compared to stricter approaches such as Family-Wise Error (FWE) correction or voxel-wise permutation testing. Additionally, while we employed permutation testing specifically to assess the significance of peak correlation (R-value), this approach does not substitute a full voxel-wise permutation correction typically recommended for large-scale fMRI analyses. Future studies should employ voxel-wise permutation-based corrections or FWE methods to ensure greater statistical rigor.

Finally, the somatotopic specificity of DBS-modulated pathways was inferred from qualitative inspection of streamline projections onto cortical somatotopic maps [41]. While this observation is anatomically and clinically consistent with the cranial-cervical distribution of CCD symptoms, no formal region-based statistical analysis was conducted. This interpretation should be considered preliminary and warrants confirmation in future studies using quantitative approaches.

5. Conclusions

In conclusion, by integrating voxelwise sweet spot mapping, tract-level fiber filtering, and whole-brain network analysis, we delineated spatial and connectivity profiles associated with favorable STN-DBS outcomes in cranial-cervical dystonia. Our findings suggest that stimulation of the posterodorsolateral STN is associated with improved motor outcomes, likely through engagement of hyperdirect and indirect subthalamic pathways connected to craniofacial regions of the sensorimotor cortex. These results support the hypothesis that symptom-specific somatotopic connectivity contributes to therapeutic efficacy and underscore the importance of individualized target selection based on clinical phenotype.

CRediT authorship contribution statement

Hutao Xie: Writing – original draft, Validation, Software, Methodology, Formal analysis, Conceptualization, Writing – review & editing, Visualization, Supervision, Resources, Investigation, Data curation. **Jiansong Huang:** Writing – original draft, Validation, Methodology, Formal analysis, Conceptualization, Visualization, Software, Investigation, Data curation. **Ningfei Li:** Visualization, Software, Writing – review & editing, Validation, Methodology. **Houyou Fan:** Writing – review & editing, Validation, Resources, Investigation, Conceptualization, Writing – original draft, Supervision, Methodology, Formal analysis. **Shihang Yang:** Writing – original draft, Software, Methodology, Visualization, Project administration, Data curation, Conceptualization. **Zixiao Yin:** Visualization, Methodology, Data curation, Writing – original draft, Software, Formal analysis, Conceptualization. **Zhaoting Zheng:** Writing – original draft, Resources, Conceptualization, Software, Formal analysis. **Zehua Zhao:** Visualization, Methodology, Validation, Conceptualization. **Yin Jiang:** Software, Project administration, Writing – review & editing, Resources, Data curation. **Lin Shi:** Visualization, Conceptualization, Project administration. **Anchao Yang:** Funding acquisition, Validation, Data curation. **Fangang Meng:** Writing – original draft, Investigation, Supervision. **Guanyu Zhu:** Writing – original draft, Investigation, Software, Data curation. **Quan Zhang:** Writing – review & editing, Formal analysis, Supervision, Conceptualization. **Jianguo Zhang:** Visualization, Resources, Methodology, Formal analysis, Writing – review & editing, Supervision, Project administration, Funding acquisition, Conceptualization.

Funding

This work is supported by the National Natural Science Foundation of China (82201634, 82401713, 82301655, 82371256, T2488101 and 82171442), China, and the Postdoctoral Fellowship Program of CPSF (GZC20231742), China.

Declaration of competing interest

The authors declare that they have no known competing financial interests or personal relationships that could have appeared to influence the work reported in this paper.

Acknowledgement

The authors would like to express their sincere gratitude to Konstantin Butenko, Andreas Horn and Garance M. Meyer for their invaluable technical support and guidance throughout this study. The authors also extend their appreciation to the lead DBS team and the Slack lead DBS forum for providing their expertise and resources, which were instrumental in the successful completion of this project.

Appendix A. Supplementary data

Supplementary data to this article can be found online at <https://doi.org/10.1016/j.brs.2025.08.003>.

References

- [1] Pandey S, Sharma S. Meige's syndrome: history, epidemiology, clinical features, pathogenesis and treatment. *J Neurol Sci* 2017;372:162–70.
- [2] Wang X, Zhang C, Wang Y, Liu C, Zhao B, Zhang JG, et al. Deep brain stimulation for craniocervical dystonia (meige syndrome): a report of four patients and a literature-based analysis of its treatment effects. *Neuromodulation* 2016;19(8):818–23.
- [3] Hao Q, Wang D, OuYang J, Ding H, Wu G, Liu Z, et al. Pallidal deep brain stimulation in primary meige syndrome: clinical outcomes and psychiatric features. *J Neurol Neurosurg Psychiatry* 2020;91(12):1343–8.
- [4] Capelle HH, Weigel R, Krauss JK. Bilateral pallidal stimulation for blepharospasm–oromandibular dystonia (meige syndrome). *Neurology* 2003;60(12):2017–8.
- [5] Ostrem JL, Markun LC, Glass GA, Racine CA, Volz MM, Heath SL, et al. Effect of frequency on subthalamic nucleus deep brain stimulation in primary dystonia. *Park Relat Disord* 2014;20(4):432–8.
- [6] Zhan S, Sun F, Pan Y, Liu W, Huang P, Cao C, et al. Bilateral deep brain stimulation of the subthalamic nucleus in primary meige syndrome. *J Neurosurg* 2018;128(3):897–902.
- [7] Hao QP, Zheng WT, Zhang ZH, Liu YZ, Ding H, OuYang J, et al. Subthalamic nucleus deep brain stimulation in primary meige syndrome: motor and non-motor outcomes. *Eur J Neurol* 2024;31(2):e16121.
- [8] Xie H, Shan M, Wang S, Diao Y, Zhang Q, Gan Y, et al. Deep brain stimulation of the subthalamic nucleus for primary meige syndrome: clinical outcomes and predictive factors. *J Neurosurg* 2024;140(6):1650–63.
- [9] Yao C, Horn A, Li N, Lu Y, Fu Z, Wang N, et al. Post-operative electrode location and clinical efficacy of subthalamic nucleus deep brain stimulation in meige syndrome. *Park Relat Disord* 2019;58:40–5.
- [10] Zheng W, Hao Q, Chen X, Liu Y, Zhang Z, Li Z, et al. Subthalamic nucleus deep brain stimulation for meige syndrome: long-term outcomes and analysis of prognostic factors. *Neurosurgery* 2025;96(6):1282–9.
- [11] Hollunder B, Ostrem JL, Sahin IA, Rajamani N, Oxenford S, Butenko K, et al. Mapping dysfunctional circuits in the frontal cortex using deep brain stimulation. *Nat Neurosci* 2024;27(3):573–86.
- [12] Horn A, Reich MM, Ewert S, Li N, Al-Fatly B, Lange F, et al. Optimal deep brain stimulation sites and networks for cervical vs. generalized dystonia. *Proc Natl Acad Sci U S A* 2022;119(14):e2114985119.
- [13] Butenko K, Neudorfer C, Dembek TA, Hollunder B, Meyer GM, Li N, et al. Engaging dystonia networks with subthalamic stimulation. *Proc Natl Acad Sci U S A* 2025;122(2):e2417617122.
- [14] Neudorfer C, Butenko K, Oxenford S, Rajamani N, Achtzehn J, Goede L, et al. Lead-DBS v3.0: mapping deep brain stimulation effects to local anatomy and global networks. *Neuroimage* 2023;268:119862.
- [15] Albanese A, Bhatia K, Bressman SB, Delong MR, Fahn S, Fung VS, et al. Phenomenology and classification of dystonia: a consensus update. *Mov Disord* 2013;28(7):863–73.
- [16] Avants BB, Epstein CL, Grossman M, Gee JC. Symmetric diffeomorphic image registration with cross-correlation: evaluating automated labeling of elderly and neurodegenerative brain. *Med Image Anal* 2008;12(1):26–41.
- [17] Horn A, Li N, Dembek TA, Kappel A, Boulay C, Ewert S, et al. Lead-DBS v2: towards a comprehensive pipeline for deep brain stimulation imaging. *Neuroimage* 2019;184:293–316.
- [18] Fonov V, Evans AC, Botteron K, Almlı CR, McKinstry RC, Collins DL, et al. Unbiased average age-appropriate atlases for pediatric studies. *Neuroimage* 2011;54(1):313–27.
- [19] Ewert S, Horn A, Finkel F, Li N, Kuhn AA, Herrington TM. Optimization and comparative evaluation of nonlinear deformation algorithms for atlas-based segmentation of DBS target nuclei. *Neuroimage* 2019;184:586–98.

- [20] Vogel D, Shah A, Coste J, Lemaire JJ, Wardell K, Hemm S. Anatomical brain structures normalization for deep brain stimulation in movement disorders. *Neuroimage Clin* 2020;27:102271.
- [21] Husch A, M VP, Gemmar P, Goncalves J, Hertel F. PaCER - a fully automated method for electrode trajectory and contact reconstruction in deep brain stimulation. *Neuroimage Clin* 2018;17:80–9.
- [22] Ewert S, Plettig P, Li N, Chakravarty MM, Collins DL, Herrington TM, et al. Toward defining deep brain stimulation targets in MNI space: a subcortical atlas based on multimodal MRI, histology and structural connectivity. *Neuroimage* 2018;170: 271–82.
- [23] Chakravarty MM, Bertrand G, Hodge CP, Sadikot AF, Collins DL. The creation of a brain atlas for image guided neurosurgery using serial histological data. *Neuroimage* 2006;30(2):359–76.
- [24] Vorwerk J, Oostenveld R, Piastra MC, Magyari L, Wolters CH. The FieldTrip-SimBio pipeline for EEG forward solutions. *Biomed Eng Online* 2018;17(1):37.
- [25] Astrom M, Diczfalusy E, Martens H, Wardell K. Relationship between neural activation and electric field distribution during deep brain stimulation. *IEEE Trans Biomed Eng* 2015;62(2):664–72.
- [26] Reich MM, Horn A, Lange F, Roothans J, Paschen S, Runge J, et al. Probabilistic mapping of the antidysonstic effect of pallidal neurostimulation: a multicentre imaging study. *Brain* 2019;142(5):1386–98.
- [27] Rios AS, Oxenford S, Neudorfer C, Butenko K, Li N, Rajamani N, et al. Optimal deep brain stimulation sites and networks for stimulation of the fornix in alzheimer's disease. *Nat Commun* 2022;13(1):7707.
- [28] Vasques X, Cif L, Hess O, Gavarini S, Mennessier G, Coubes P. Stereotactic model of the electrical distribution within the internal globus pallidus during deep brain stimulation. *J Comput Neurosci* 2009;26(1):109–18.
- [29] Meyer GM, Hollunder B, Li N, Butenko K, Dembek TA, Hart L, et al. Deep brain stimulation for obsessive-compulsive disorder: optimal stimulation sites. *Biol Psychiatry* 2024;96(2):101–13.
- [30] Elias GJB, Germann J, Joel SE, Li N, Horn A, Boutet A, et al. A large normative connectome for exploring the tractographic correlates of focal brain interventions. *Sci Data* 2024;11(1):353.
- [31] Petersen MV, Mlakar J, Haber SN, Parent M, Smith Y, Strick PL, et al. Holographic reconstruction of axonal pathways in the human brain. *Neuron* 2019;104(6): 1056–1064 e3.
- [32] Fan H, Guo Z, Jiang Y, Xue T, Yin Z, Xie H, et al. Optimal subthalamic stimulation sites and related networks for freezing of gait in parkinson's disease. *Brain Commun* 2023;5(5):fcad238.
- [33] Li N, Hollunder B, Baldermann JC, Kibleur A, Treu S, Akram H, et al. A unified functional network target for deep brain stimulation in obsessive-compulsive disorder. *Biol Psychiatry* 2021;90(10):701–13.
- [34] Li N, Baldermann JC, Kibleur A, Treu S, Akram H, Elias GJB, et al. A unified connectomic target for deep brain stimulation in obsessive-compulsive disorder. *Nat Commun* 2020;11(1):3364.
- [35] Baldermann JC, Melzer C, Zapf A, Kohl S, Timmermann L, Tittgemeyer M, et al. Connectivity profile predictive of effective deep brain stimulation in obsessive-compulsive disorder. *Biol Psychiatry* 2019;85(9):735–43.
- [36] Cohen A, Soussand L, McManus P, Fox M. GSP1000 Preprocessed Connectome. Harvard Dataverse 2020;V3. <https://doi.org/10.7910/DVN/LXIKS>.
- [37] Alkemade A, Bazin PL, Balesar R, Pine K, Kirilina E, Moller HE, et al. A unified 3D map of microscopic architecture and MRI of the human brain. *Sci Adv* 2022;8(17): eabj7892.
- [38] Nambu A. Somatotopic organization of the primate basal ganglia. *Front Neuroanat* 2011;5:26.
- [39] Mundinger F. New stereotactic treatment of spasmotic torticollis with a brain stimulation system [author's transl]. *Med Klin* 1977;72(46):1982–6.
- [40] Hassler R, Riechert T, Mundinger F, Umbach W, Ganglberger JA. Physiological observations in stereotaxic operations in extrapyramidal motor disturbances. *Brain* 1960;83:337–50.
- [41] Penfield W, Boldrey E. Somatic motor and sensory representation in the cerebral cortex of man as studied by electrical STIMULATION1. *Brain* 1937;60(4):389–443.
- [42] Gill JS, Nguyen MX, Hull M, van der Heijden ME, Nguyen K, Thomas SP, et al. Function and dysfunction of the dystonia network: an exploration of neural circuits that underlie the acquired and isolated dystonias. *Dystonia* 2023;2.
- [43] Corp DT, Greenwood CJ, Morrison-Ham J, Pullinen J, McDowall GM, Younger EFP, et al. Clinical and structural findings in patients with lesion-induced dystonia: descriptive and quantitative analysis of published cases. *Neurology* 2022;99(18): e1957–67.
- [44] Liuzzi D, Gigante AF, Leo A, Defazio G. The anatomical basis of upper limb dystonia: lesson from secondary cases. *Neurol Sci* 2016;37(9):1393–8.
- [45] Peterson DA, Sejnowski TJ. A dynamic circuit hypothesis for the pathogenesis of blepharospasm. *Front Comput Neurosci* 2017;11:11.
- [46] Defazio G, Hallett M, Jinnah HA, Conte A, Berardelli A. Blepharospasm 40 years later. *Mov Disord* 2017;32(4):498–509.
- [47] Corp DT, Joutsa J, Darby RR, Delnooz CCS, van de Warrenburg BPC, Cooke D, et al. Network localization of cervical dystonia based on causal brain lesions. *Brain* 2019;142(6):1660–74.
- [48] Grimm K, Prilop L, Schon G, Gelderblom M, Misselhorn J, Gerloff C, et al. Cerebellar modulation of sensorimotor associative plasticity is impaired in cervical dystonia. *Mov Disord* 2023;38(11):2084–93.
- [49] Conte A, Belvisi D, De Bartolo MI, Manzo N, Cortese FN, Tartaglia M, et al. Abnormal sensory gating in patients with different types of focal dystonias. *Mov Disord* 2018;33(12):1910–7.
- [50] Manzo N, Ginatempo F, Belvisi D, Defazio G, Conte A, Deriu F, et al. Pathophysiological mechanisms of oromandibular dystonia. *Clin Neurophysiol* 2022;134:73–80.
- [51] Ramos VF, Karp BI, Hallett M. Tricks in dystonia: ordering the complexity. *J Neurol Neurosurg Psychiatry* 2014;85(9):987–93.
- [52] Greene PE, Bressman S. Exteroceptive and interoceptive stimuli in dystonia. *Mov Disord* 1998;13(3):549–51.
- [53] Quattrone A, Latorre A, Magrinelli F, Mulroy E, Rajan R, Neo RJ, et al. A reflection on motor overflow, mirror phenomena, synkinesia and entrainment. *Mov Disord Clin Pract* 2023;10(9):1243–52.
- [54] Koketsu D, Chiken S, Hisatsune T, Miyachi S, Nambu A. Elimination of the cortico-subthalamic hyperdirect pathway induces motor hyperactivity in mice. *J Neurosci* 2021;41(25):5502–10.
- [55] Nambu A, Chiken S, Sano H, Hatanaka N, Obeso JA. Dynamic activity model of movement disorders: the fundamental role of the hyperdirect pathway. *Mov Disord* 2023;38(12):2145–50.
- [56] Horn A, Ewert S, Alho EJL, Axer M, Heinsen H, Fonoff ET, et al. Teaching NeuroImages: in vivo visualization of edinger comb and wilson pencils. *Neurology* 2019;92(14):e1663–4.
- [57] Oswal A, Cao C, Yeh CH, Neumann WJ, Gratwickie J, Akram H, et al. Neural signatures of hyperdirect pathway activity in parkinson's disease. *Nat Commun* 2021;12(1):5185.
- [58] Calabresi P, Picconi B, Tozzi A, Ghiglieri V, Di Filippo M. Direct and indirect pathways of basal ganglia: a critical reappraisal. *Nat Neurosci* 2014;17(8): 1022–30.
- [59] Gianni C, Pasqua G, Ferrazzano G, Tommasin S, De Bartolo MI, Petsas N, et al. Focal dystonia: functional connectivity changes in cerebellar-basal ganglia-cortical circuit and preserved global functional architecture. *Neurology* 2022;98(14): e1499–509.
- [60] Gianni C, Piervincenzi C, Belvisi D, Tommasin S, De Bartolo MI, Ferrazzano G, et al. Cortico-subcortical white matter bundle changes in cervical dystonia and blepharospasm. *Biomedicines* 2023;11(3).
- [61] Nguyen P, Kelly D, Glickman A, Argaw S, Shelton E, Peterson DA, et al. Abnormal neural responses during reflexive blinking in blepharospasm: an event-related functional MRI study. *Mov Disord* 2020;35(7):1173–80.
- [62] Huang XF, Hao XQ, Yin XX, Ren L, Wang D, Jin F, et al. Functional connectivity alterations in the frontoparietal network and sensorimotor network are associated with behavioral heterogeneity in blepharospasm. *Front Neurol* 2023;14:1273935.
- [63] Ginatempo F, Manzo N, Loi N, Belvisi D, Cutrona C, Conte A, et al. Abnormalities in the face primary motor cortex in oromandibular dystonia. *Clin Neurophysiol* 2023; 151:151–60.
- [64] Hao X, Huang X, Yin X, Wang HY, Lu R, Liang Z, et al. Elucidation of the mechanism underlying impaired sensorimotor gating in patients with primary blepharospasm using prepulse inhibition. *Front Neurol* 2023;14:1105483.
- [65] Neychev VK, Gross RE, Lehericy S, Hess EJ, Jinnah HA. The functional neuroanatomy of dystonia. *Neurobiol Dis* 2011;42(2):185–201.
- [66] Hollunder B, Rajamani N, Siddiqi SH, Finke C, Kuhn AA, Mayberg HS, et al. Toward personalized medicine in connectomic deep brain stimulation. *Prog Neurobiol* 2022;210:102211.
- [67] Horn A, Fox MD. Opportunities of connectomic neuromodulation. *Neuroimage* 2020;221:117180.
- [68] Neumann WJ, Horn A, Kuhn AA. Insights and opportunities for deep brain stimulation as a brain circuit intervention. *Trends Neurosci* 2023;46(6):472–87.
- [69] Hart MG, Polyhronopoulos N, Sandhu MK, Honey CR. Deep brain stimulation improves symptoms of Spasmodic dysphonia through targeting of thalamic sensorimotor connectivity. *Neurosurgery* 2024;94(6):1291–300.
- [70] Phukan J, Albanese A, Gasser T, Warner T. Primary dystonia and dystonia-plus syndromes: clinical characteristics, diagnosis, and pathogenesis. *Lancet Neurol* 2011;10(12):1074–85.
- [71] Hallett M. Pathophysiology of writer's cramp. *Hum Mov Sci* 2006;25(4–5):454–63.
- [72] Baizabal-Carvallo JF, Hallett M, Jankovic J. Pathogenesis and pathophysiology of functional (psychogenic) movement disorders. *Neurobiol Dis* 2019;127:32–44.
- [73] Ikeda A. [Human supplementary motor area: a role in voluntary movements and its clinical significance]. *Rinsho Shinkeigaku* 2007;47(11):723–6.
- [74] Cho HJ, Waugh R, Wu T, Panyakaew P, Mente K, Urbano D, et al. Role of supplementary motor area in cervical dystonia and sensory tricks. *Sci Rep* 2022;12(1):21206.
- [75] Xu J, Zhang X, Cheng Q, Zhang H, Zhong L, Luo Y, et al. Abnormal supplementary motor areas are associated with idiopathic and acquired blepharospasm. *Park Relat Disord* 2024;121:106029.
- [76] Dresel C, Haslinger B, Castrop F, Wohlschlaeger AM, Ceballos-Baumann AO. Silent event-related fMRI reveals deficient motor and enhanced somatosensory activation in orofacial dystonia. *Brain* 2006;129(Pt 1):36–46.
- [77] Guehl D, Cuny E, Ghorayeb I, Michelet T, Bioulac B, Burbaud P. Primate models of dystonia. *Prog Neurobiol* 2009;87(2):118–31.
- [78] Cuny E, Ghorayeb I, Guehl D, Escola L, Bioulac B, Burbaud P. Sensory motor mismatch within the supplementary motor area in the dystonic monkey. *Neurobiol Dis* 2008;30(2):151–61.
- [79] Kaji R, Bhatia K, Graybiel AM. Pathogenesis of dystonia: is it of cerebellar or basal ganglia origin? *J Neurol Neurosurg Psychiatry* 2018;89(5):488–92.
- [80] Liu J, Li L, Li Y, Wang Q, Liu R, Ding H. Regional metabolic and network changes in meige syndrome. *Sci Rep* 2021;11(1):15753.
- [81] Liu B, Mao Z, Cui Z, Ling Z, Xu X, He K, et al. Cerebellar gray matter alterations predict deep brain stimulation outcomes in meige syndrome. *Neuroimage Clin* 2023;37:103316.

- [82] Yang J, Luo C, Song W, Guo X, Zhao B, Chen X, et al. Diffusion tensor imaging in blepharospasm and blepharospasm-oromandibular dystonia. *J Neurol* 2014;261(7):1413–24.
- [83] Persing JA, Muir A, Becker DG, Jankovic JJ, Anderson RL, Edlich RF. Blepharospasm-oromandibular dystonia associated with a left cerebellopontine angle meningioma. *J Emerg Med* 1990;8(5):571–4.
- [84] Fagan M, Scorr L, Bernhardt D, Hess EJ, Perlmuter JS, Pardo CA, et al. Neuropathology of blepharospasm. *Exp Neurol* 2021;346:113855.
- [85] Ilinsky I, Horn A, Paul-Gilloteaux P, Gressens P, Verney C, Kultas-Ilinsky K. Human motor thalamus reconstructed in 3D from continuous sagittal sections with identified subcortical afferent territories. *eNeuro* 2018;5(3).
- [86] Parent A, De Bellefeuille L. Organization of efferent projections from the internal segment of globus pallidus in primate as revealed by fluorescence retrograde labeling method. *Brain Res* 1982;245(2):201–13.
- [87] Tewari A, Fremont R, Khodakhah K. It's not just the basal ganglia: cerebellum as a target for dystonia therapeutics. *Mov Disord* 2017;32(11):1537–45.
- [88] Evans AC, Janke AL, Collins DL, Baillet S. Brain templates and atlases. *Neuroimage* 2012;62(2):911–22.
- [89] Edlow BL, Mareyam A, Horn A, Polimeni JR, Witzel T, Tisdall MD, et al. 7 tesla MRI of the ex vivo human brain at 100 micron resolution. *Sci Data* 2019;6(1):244.